traveling wave is narrower, and the phase velocity, which is related to Φ by $V_p = (kh/\Phi)(b/h)V_0$, is lower. Comparison with the result obtained for a single-row Yagi structure shows that the coupling effect at $U = 2h$ causes less than a 2-percent change in the K–β diagram.

The theoretical result has been verified by experiments [10], as shown in Fig. 2. Theory also predicts that the field intensity in the transverse direction (x direction in Fig. 1) decays exponentially. This is a typical characteristic of a guided wave. In Fig. 3 the measured field intensity is shown to decay at approximately 35 dB per wavelength in the x direction. This shows that the level of mutual coupling in the transverse direction is rather low when the arrays are separated by at least one wavelength.

References

[1] L. C. Shen, "Numerical analysis of wave propagation on a periodic linear array," *IEEE Trans. Antennas Propagat.*, vol. AP-19, pp. 289–292, 1971.

[2] K. Yoshimura and S. Tokumaru, "Calculated phase constant of coupled Yagi arrays," *Electronics and Communications in Japan*, vol. 54-B, no. 10, pp. 94–100, 1971.

[3] L. C. Shen, "Characteristics of propagating waves on Yagi–Uda structure," *IEEE Trans. Microwave Theory Tech.*, vol. MTT-19, pp. 536–542, 1971.

[4] R. J. Mailloux, "Antenna and wave theories of infinite Yagi–Uda arrays," *IEEE Trans. Antennas Propagat.*, vol. AP-13, pp. 499–506, 1965.

[5] L. C. Shen, H. D. Cubley, and D. S. Eggers, "Measurement of the propagating waves on Yagi–Uda array," *IEEE Trans. Antennas Propagat.*, vol. AP-19, pp. 776–779, 1971.

[6] L. C. Shen, "Possible new applications of periodic linear arrays," *IEEE Trans. Antennas Propagat.*, vol. AP-18, pp. 698–699, 1970.

[7] R. W. P. King, *The Theory of Linear Antennas*. Cambridge, MA: Harvard University Press, 1956, p. 422.

[8] R. F. Harrington, *Field Computation by Moment Methods*. New York: MacMillan, 1968.

[9] V. W. H. Chang and R. W. P. King, "On two arbitrarily located identical parallel antennas," *IEEE Trans. Antennas Propagat.*, vol. AP-16, pp. 309–317, 1968.

[10] C. C. Lee, "Coupled Yagi–Uda arrays of dipoles," Ph.D. dissertation, University of Houston, Houston, TX, 1976.

Coupling of Circuit Structures to Magnetostatic Modes of Ferromagnetic Resonators

NICOLAS J. MOLL, MEMBER, IEEE

Abstract—**The coupling between a current-carrying circuit structure and the magnetostatic modes of a general ferromagnet, such as a YIG resonator, is examined. A small-signal theory is presented that describes the excitation of an arbitrary mode in terms of an effective susceptibility matrix; this description leads to a simple method for calculating the z parameters of the resonator and coupling structure combination. This result is tested by comparison with other theory and with experiment. Applied to the case of a uniform field exciting the uniform mode of an ellipsoidal resonator, it reduces to Carter's well-known formula. Applied to the case of a particular nonuniform field exciting the main mode of a thin square resonator, it predicts the experimental finding that the coupling strength depends only on the resonator's thickness. This last case illustrates the extended generality of our result which allows the treatment of situations where the RF magnetization and field are not uniform.**

Nomenclature

$\hat{a}_m$	Unit vector in the direction of dc magnetization.
$\hat{a}_x,\hat{a}_y,\hat{a}_z$	Coordinate axis unit vectors.
H	Total magnetic field.
h_d	RF demagnetizing field.
h_e	Circuit induced field.
H_i	Magnitude of dc field inside resonator.
H_0	Magnitude of applied dc magnetic field.
k_p	Magnetic coupling function for port p.
k_{pu}	Decomposition of k_p on Ψ_{ur} and Ψ_{ui}.
$k_{pu}^{\dagger}$	Adjoint of the matrix k_{pu}.
m	RF magnetization.
M	Total magnetization.
M_s	Saturation magnetization.
m_u	Complex amplitude of the uth eigenfunction.
S_Ω	Surface enclosing the volume Ω.
V	Resonator volume.
γ	Gyromagnetic ratio.
δ_{uv}	Kronecker symbol.
χ_u	Matrix of susceptibilities for the uth mode.
Ψ_u	uth eigenfunction.
Ψ_{ur},Ψ_{ui}	Normalized real and imaginary parts of Ψ_u.
$\Delta\omega$	Unloaded radian bandwidth of resonator.
ω_M	Magnetization frequency γM_s.
Ω	All space excluding metallic conductors.

Manuscript received December 1, 1976; revised April 15, 1977.

The author is with the Solid State Laboratory, Hewlett-Packard Laboratories, Palo Alto, CA 94304.

Introduction

A FERROMAGNETIC resonator was first used in a practical circuit—a YIG sphere filter gyrator—by Degrasse [1]. The problem of coupling a circuit, via induced magnetic fields, to an ellipsoidal resonator was analyzed

shortly thereafter by Carter [2]. His analysis, based on simulation of the ferromagnetic resonator with current loops, contains two important restrictions: currents flowing in the coupling structure must produce a uniform RF field in the vicinity of the resonator, and only the uniform precessional mode must be excited in the resonator. Carter's results are therefore unsuited for application to problems relating to disk resonators since the coupling structure generally produces a nonuniform RF field within the disk, and since disk resonators will not support the uniform precessional mode [3].

We have worked out a more general theory which predicts the impedance due to any magnetostatic mode or modes of any insulating ferromagnet coupled to any circuit structure. The theory relies on deduction of the z parameters from the complex power flow out of the coupling structure. By calculating this power flow as an appropriate volume integral, we are able to avoid the artifice of replacing the resonator with a current loop, a procedure both confusing and difficult to justify in the case of nonuniform field and magnetization. In order to calculate this volume integral, we need to review some rudimentary properties of the magnetostatic modes, and to show that most terms within the integral are zero. Once these preliminaries are taken care of, the z parameters are obtained quite directly.

Magnetostatic Modes

A ferromagnetic resonator has a sizable number of possible resonant modes. For a given resonator, many of these modes will behave independently of either exchange or electromagnetic propagation effects, and thus earn the name of magnetostatic mode [4]–[6]. In the absence of anisotropy effects, they are solutions of the lossless magnetostatic equations of motion:

$$\partial \boldsymbol{M}/\partial t = \gamma \boldsymbol{M} \times \boldsymbol{H} \tag{1a}$$

$$\nabla \times \boldsymbol{H} = 0 \tag{1b}$$

$$\nabla \cdot (\boldsymbol{H} + \boldsymbol{M}) = 0. \tag{1c}$$

When anisotropy is important, it can sometimes be accounted for by adding an effective anisotropy field to the dc field H_i. Our reasoning is general enough to include this possibility.

We will now write the small-signal versions of (1), including a Bloch–Bloembergen loss term $\frac{1}{2}\Delta\omega$ [7] and an RF driving field $\boldsymbol{h}_e$. The unit vector $\hat{\boldsymbol{a}}_m$ gives the direction of the dc magnetization and internal magnetic field. As indicated in Fig. 1, its direction is arbitrary and may vary throughout the sample volume. Then in phasor notation,

$$(j\omega + \tfrac{1}{2}\Delta\omega)\boldsymbol{m} = \gamma M_s \hat{\boldsymbol{a}}_m \times [\boldsymbol{h}_d + \boldsymbol{h}_e - (H_i/M_s)\boldsymbol{m}]. \tag{2}$$

The equations of motion can be reduced to an eigenfunction problem by using a Green's function solution of (1c):

$$\boldsymbol{h}_d = \nabla \mathcal{G} \nabla \cdot \boldsymbol{m} \tag{3a}$$

where the Green's operator has the general form

$$\mathcal{G}f(\boldsymbol{r}) = \int_\Omega K(\boldsymbol{r},\boldsymbol{r}_1) f(\boldsymbol{r}_1)\, dV_1. \tag{3b}$$

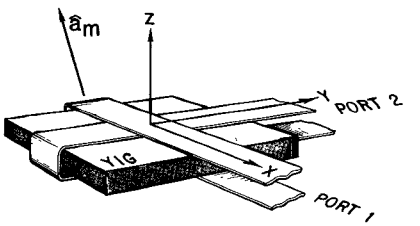

Fig. 1. A typical resonator coupling-structure combination. The case shown is an $l \times l$ square resonator in a bandpass filter arrangement. The unit vector $\hat{\boldsymbol{a}}_m$ indicates the direction of the dc magnetization, which may vary with position.

The kernel $K(\boldsymbol{r},\boldsymbol{r}_1)$ depends on the coupling structure, because the normal derivative of K must be zero at metallic boundaries. Regardless of the exact form of $\mathcal{G}$, (2) becomes

$$(j\omega + \tfrac{1}{2}\Delta\omega)\boldsymbol{m} = \mathcal{L}(\boldsymbol{m}) + \gamma M_s \hat{\boldsymbol{a}}_m \times \boldsymbol{h}_e \tag{4a}$$

where

$$\mathcal{L}(\boldsymbol{m}) = \gamma M_s \hat{\boldsymbol{a}}_m \times [\nabla \mathcal{G} \nabla \cdot - (H_i/M_s)]\boldsymbol{m}. \tag{4b}$$

The magnetostatic modes are then the eigenfunctions of the operator $\mathcal{L}$. We will write the uth eigenfunction as $\boldsymbol{\Psi}_u$; its corresponding eigenfrequency is ω_u, taken to be positive. An examination of (4a) shows that in addition to the set of eigenfunctions $\boldsymbol{\Psi}_u$ with positive eigenfrequencies, the set of complex conjugates $\boldsymbol{\Psi}_u^*$ are also eigenfunctions, but with negative eigenfrequencies. As a matter of convenience, we will write $\boldsymbol{\Psi}_u^*$ as $\boldsymbol{\Psi}_{-u}$.

As shown in Appendix I, these modes obey the rather unusual orthogonality relation

$$\frac{1}{jV}\int_V \boldsymbol{\Psi}_u^* \times \boldsymbol{\Psi}_v \cdot \hat{\boldsymbol{a}}_m\, dV = \pm\delta_{uv} \tag{5}$$

with suitable normalization. The minus sign on the right-hand side is chosen when $u < 0$.

We can now predict the exact RF magnetization produced by an arbitrary exciting field, subject to the assumption that the magnetization can be expanded as a sum of the eigenfunctions; that is,

$$\boldsymbol{m} = \sum_1^\infty (m_u \boldsymbol{\Psi}_u + m_{-u}\boldsymbol{\Psi}_{-u}). \tag{6}$$

Some observations about the validity of this assumption are in order.

From a mathematical standpoint, (6) can be written down without hesitation if the eigenfunctions form a complete set in the space of functions that map position within the resonator into a complex vector perpendicular to $\hat{\boldsymbol{a}}_m$. For specific cases such as a sphere in free space in a uniform field, the eigenfunctions clearly have this property. It is not, however, obvious from the general form of $\mathcal{L}$ that they invariably do, and the assumption should be checked case by case.

From a physical standpoint, (6) simply says that the magnetization is a superposition of the magnetostatic modes. In most practical problems, this is apparently the

case; then the mode spectrum need not be examined for completeness.

Substituting (6) into (4) and applying (5), we then obtain

$$(\omega \pm \omega_u - \tfrac{1}{2}j\Delta\omega)m_{\mp u} = \pm\frac{\gamma M_s}{V}\int_V \boldsymbol{h}_e \cdot \boldsymbol{\Psi}_{\pm u}\, dV \qquad (7)$$

where $u > 0$. At this point, it becomes convenient to introduce a different representation than the eigenfunctions. Posing

$$\boldsymbol{\Psi}_{ur} = \frac{\boldsymbol{\Psi}_u + \boldsymbol{\Psi}_{-u}}{\sqrt{2}} \qquad \boldsymbol{\Psi}_{ui} = \frac{\boldsymbol{\Psi}_u - \boldsymbol{\Psi}_{-u}}{j\sqrt{2}} \qquad (8a)$$

$$m_{ur} = \frac{m_u + m_{-u}}{\sqrt{2}} \qquad m_{ui} = j\frac{m_u - m_{-u}}{\sqrt{2}} \qquad (8b)$$

we have

$$\boldsymbol{m} = \sum_1^\infty m_{ur}\boldsymbol{\Psi}_{ur} + m_{ui}\boldsymbol{\Psi}_{ui}. \qquad (8c)$$

Then

$$\begin{pmatrix} m_{ur} \\ m_{ui} \end{pmatrix} = \begin{pmatrix} \chi_{urr} & \chi_{uri} \\ \chi_{uir} & \chi_{uii} \end{pmatrix}\begin{pmatrix} h_{ur} \\ h_{ui} \end{pmatrix} \qquad (9a)$$

where

$$\begin{pmatrix} h_{ur} \\ h_{ui} \end{pmatrix} = \frac{1}{V}\int_V \begin{pmatrix} \boldsymbol{h}_e \cdot \boldsymbol{\Psi}_{ur} \\ \boldsymbol{h}_e \cdot \boldsymbol{\Psi}_{ui} \end{pmatrix} dV \qquad (9b)$$

and

$$\chi_{urr} = \chi_{uii} = \frac{\omega_u\omega_M}{\omega_u^2 - (\omega - \frac{1}{2}j\Delta\omega)^2} \qquad (9c)$$

$$-\chi_{uri} = \chi_{uir} = \frac{j(\omega - \frac{1}{2}j\Delta\omega)\omega_M}{\omega_u^2 - (\omega - \frac{1}{2}j\Delta\omega)^2}. \qquad (9d)$$

These equations constitute a complete description of the behavior of the uth magnetostatic mode. They closely resemble the effective susceptibility description of the uniform precessional mode of an ellipsoidal resonator. The susceptibility tensor is in fact the same except that the resonant frequency is that of the uth mode. However, the driving field and magnetization, rather than being projected on coordinate axes, are projected against the functions $\boldsymbol{\Psi}_{ur}$ and $\boldsymbol{\Psi}_{ui}$. This result was qualitatively anticipated by Dillon when he observed that a given mode will or will not be excited by a given RF field distribution depending on "its projection on the transverse magnetization of the mode in question" [5].

Circuit–Resonator Power Flow

According to Poynting's theorem, the instantaneous power flowing out of the coupling structure is

$$P(t) = \mu_0\int_\Omega \left[\frac{\partial}{\partial t}(\boldsymbol{h}(t) + \boldsymbol{m}(t))\right] \cdot \boldsymbol{h}(t)\, dV \qquad (10)$$

in the magnetostatic approximation. The volume of integration is all space excluding metallic conductors, and thus includes fringing demagnetization fields. For the case of field quantities varying in time as $e^{j\omega t}$, we can most conveniently use the complex power

$$P = \text{average power} + j \cdot \text{reactive power} \qquad (11a)$$

$$= \tfrac{1}{2}j\omega\mu_0\int_\Omega (\boldsymbol{h} + \boldsymbol{m}) \cdot \boldsymbol{h}^*\, dV. \qquad (11b)$$

Properly speaking, $\boldsymbol{h}$ is the total RF magnetic field $\boldsymbol{h}_e + \boldsymbol{h}_d$. However, the terms $(\boldsymbol{m} + \boldsymbol{h}) \cdot \boldsymbol{h}_d^*$ and $\boldsymbol{h}_d \cdot \boldsymbol{h}_e^*$ make no contribution to the integral (see Appendix II) so

$$P = \tfrac{1}{2}j\omega\mu_0\int_\Omega [\boldsymbol{h}_e \cdot \boldsymbol{h}_e^* + \boldsymbol{m} \cdot \boldsymbol{h}_e^*]\, dV. \qquad (12a)$$

The power from the first term is imaginary; it corresponds to the reactive power flow in the ordinary inductances of the circuit. If we neglect this term, we have simply

$$P = \tfrac{1}{2}j\omega\mu_0\int_V \boldsymbol{m} \cdot \boldsymbol{h}_e^*\, dV. \qquad (12b)$$

Using the result of the preceding section, we can write the power flow in an n-port structure in terms of port currents; the resulting expression then allows the deduction of the z parameters of the n-port.

The total external magnetic field induced by an n-port coupling structure is

$$\boldsymbol{h}_e = \sum_{p=1}^n i_p\boldsymbol{k}_p \qquad (13)$$

where $i_p\boldsymbol{k}_p$ is the magnetic field induced by a current i_p flowing into port p. Combining (8c), (9a), (9b), (12b), and (13), we find

$$P = \tfrac{1}{2}j\omega\mu_0 V\sum_{u,p,q} i_p^*\boldsymbol{k}_{pu}^\dagger\chi_u\boldsymbol{k}_{qu}i_q \qquad (14a)$$

where the coupling matrix for port q and mode u is

$$\boldsymbol{k}_{qu} = \frac{1}{V}\int_V \begin{pmatrix} \boldsymbol{k}_q \cdot \boldsymbol{\Psi}_{ur} \\ \boldsymbol{k}_q \cdot \boldsymbol{\Psi}_{ui} \end{pmatrix} dV. \qquad (14b)$$

The complex power flowing into an n-port network is

$$P = \tfrac{1}{2}\sum_p i_p^* v_p \qquad (15a)$$

$$= \tfrac{1}{2}\sum_{p,q} i_p^* Z_{pq} i_q \qquad (15b)$$

so the z parameters of the ferromagnetic device are

$$Z_{pq} = j\omega\mu_0 V\sum_u \boldsymbol{k}_{pu}^\dagger\chi_u\boldsymbol{k}_{qu}. \qquad (16)$$

A glance at the original power expression (12a) shows that when the circuit inductance is not neglected

$$Z_{pq} = j\omega\left[L_{pq} + \mu_0 V\sum_u \boldsymbol{k}_{pu}^\dagger\chi_u\boldsymbol{k}_{qu}\right] \qquad (17)$$

where L_{pq} is the appropriate self or mutual inductance. These are the z parameters of a collection of series connected n-ports; the coupling inductances are represented by one n-port, and each magnetostatic mode by another. Fig. 2 indicates this arrangement for a two-port circuit.

Equations (14b) and (17) are the main result of this paper;

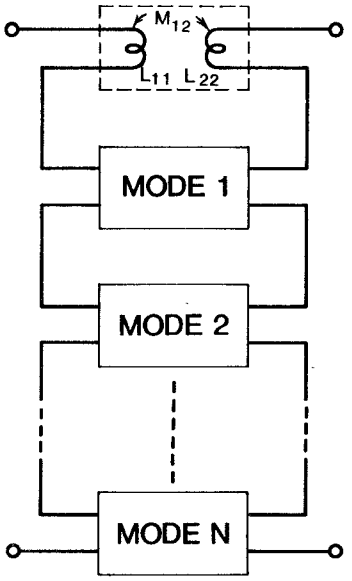

Fig. 2. The connection of single-mode two-ports into an equivalent circuit of a general ferromagnetic two-port.

in principle, they permit the calculation of the z parameters of any coupling structure and ferromagnetic resonator combination, provided that we know the spatial dependence and resonant frequencies of the excited eigenfunctions and the spatial dependence of the coupler-induced field in the vicinity of the resonator.

Applications

The theory just presented can be tested by applying it to special cases. Carter's theory covers the problem of coupling to the uniform mode of a spherical resonator; we have experimental coupling data on two configurations of flat resonators. In this section we compare these results with our own theoretical predictions.

Uniform Mode of a Sphere: Consider a YIG sphere coupled to two crossed loops perpendicular to the x and y axes. Suppose that the field produced by the loops is uniform within the sphere and that only the uniform mode is excited; this is the case considered by Carter [2], [8] and the most commonly used configuration of YIG resonators. The eigenfunction corresponding to the uniform mode is just

$$\Psi_1 = (\hat{a}_x + j\hat{a}_y)/\sqrt{2} \tag{18}$$

with an eigenfrequency $\omega_1 = \gamma H_0$. Thus

$$\Psi_{1r} = \hat{a}_x \qquad \Psi_{1i} = \hat{a}_y \tag{19}$$

whence

$$\begin{aligned} Z_{11} &= j\omega L_{11} + j\omega\mu_0 V k_1^2 \chi_{xx} \\ Z_{22} &= j\omega L_{22} + j\omega\mu_0 V k_2^2 \chi_{yy} \\ Z_{12} &= -Z_{21} = j\omega\mu_0 V k_1 k_2 \chi_{xy}. \end{aligned} \tag{20}$$

This is identical to Carter's result.

Square Resonator in a Nonuniform Field: Consider the coupling and resonator structure in Fig. 1, a sketch of a two-port bandpass filter. The magnetic field associated with the coupling structure is more or less confined to the immediate vicinity of the coupling loops. In the case where the loops' width and spacing are small compared to a side of the resonator, the circuit-induced RF field is quite nonuniform across the face of the resonator, so the situation provides a good example of the generality of the theory. A specific test of the theory is to compare the predicted and experimentally determined coupling of the structure; this is easily done in terms of the circuit's external Q, which can be determined from a simple bandwidth and insertion loss measurement.

We will limit our considerations to frequencies near the main resonance; there are no modes degenerate to the main resonance that will be coupled to the circuit, so only the main mode will be excited. If the RF magnetization is unpinned [3], the main resonance eigenfunction is approximately

$$\Psi_u \approx \sqrt{2}\cos(\pi x/l)\cos(\pi y/l)(\hat{a}_x + j\hat{a}_y). \tag{21}$$

The resonator is of length l on a side, centered on the coordinates as shown in Fig. 1. Equation (21) is the first-order plane-wave approximation to the eigenfunction; in using it we ignore effects at the resonator edges, beyond assuring that Ψ_u vanishes there, and totally neglect the effect of adjacent conductors.

The coupling function k_1 can be approximated as

$$k_1 = \begin{cases} (1/W_e)\hat{a}_x, & |x| \le \frac{1}{2}W_e \\ 0, & |x| > \frac{1}{2}W_e. \end{cases} \tag{22}$$

The effective width W_e depends on the details of the coupling geometry; as long as it is small, its exact value is unimportant because it drops out of the integral of (14b), which becomes

$$k_{1u} \approx \begin{pmatrix} 4/\pi l \\ 0 \end{pmatrix} \qquad k_{2u} \approx \begin{pmatrix} 0 \\ 4/\pi l \end{pmatrix}. \tag{23}$$

The z parameters for a resonator of thickness t are then

$$Z = j16\pi^{-2}\omega\mu_0 t\chi_u. \tag{24}$$

The external Q derived from this impedance matrix is

$$Q_E = \frac{\pi^2 Z_0}{32\mu_0 t\omega_M} \tag{25}$$

when the filter is driven and terminated with impedances of Z_0.

This is an interesting result; it says that the coupling between the resonator and a narrow loop depends only on the resonator's thickness, not on its overall size. A perusal of the mathematics shows that this property is basic to any coupling structure that confines the RF driving field to a narrow strip across the resonator. A more precise representation of Ψ_u than (21), or a resonator of a shape different from a square, will change the numerical constants in (25) but its overall form should remain substantially the same. That view is supported by the data shown in Fig. 3; there, the predicted and measured external Q's are compared for filters constructed with two different size resonators, both 20 μm thick. The resonators were made, as in the next experiment,

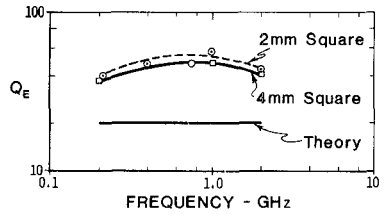

Fig. 3. A comparison of the measured and calculated Q_E for 20-μm-thick YIG resonators 2 and 4 mm square, coupled with 0.5-mm-wide strips. The coupling is nearly the same for both resonators.

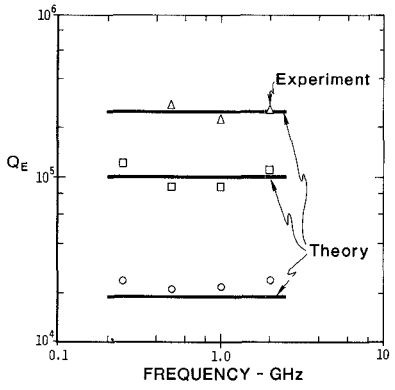

Fig. 4. A comparison of the measured and calculated Q_E for three modes of a 2-mm-diameter disk, 20 μm thick, coupled to a 50-Ω stripline. The coupling constant k_1 is $39\hat{a}_x$ in reciprocal meters. This small coupling constant, which is determined entirely by the stripline dimensions, results in the very large external Q's.

from undoped liquid-phase epitaxial YIG on a gadolinium gallium garnet substrate, and have unloaded Q's of about 1000. The data show that the external Q is indeed size independent; there is, however, a factor of two discrepancy between the measured and predicted values. This arises from the approximation involved in taking (21) as the eigenfunction.

Disk Resonator in a Uniform Field: An interesting problem to consider in this light is that of a resonator coupled to a terminated triplate stripline of dimensions somewhat larger than the resonator. Here, the effect of the metallic boundaries should be small, and the first-order plane-wave approximation should be a good quantitative description of the eigenfunction. It happens that this experiment was done with disk resonators; thus [9]

$$\Psi_u \approx \frac{J_0(s_u r/r_0)}{\sqrt{2}J_1(s_u)}(\hat{a}_x + j\hat{a}_y). \tag{26}$$

The parameter s_u is the uth root of the Bessel function J_0; Ψ_u vanishes at the edges of the disk. The external Q calculated using this approximation is

$$Q_E = \frac{s_u^2 Z_0}{4\mu_0 \omega_M V |k_1|^2}. \tag{27}$$

Fig. 4 shows the measured and calculated values of Q_E for the three lowest order modes; the quantitative agreement is good.

Conclusions

We have shown how to calculate the electrical properties of an arbitrary ferromagnetic resonator coupled to an arbitrary coupling structure. This is a considerable extension of Carter's previous work on this topic; his result strictly applies only to the uniform precessional mode of ellipsoidal resonators, and then only when this mode is driven by a uniform magnetic field. The key results of the calculation are quantitatively contained in (9), (14), and (17). These equations show that the excitation of any mode depends on the projection of the driving field against a particular representation of that mode, and on an effective matrix susceptibility of a form similar to the bulk susceptibility. These results are applied to special cases. The problem of a thin square resonator coupled to a narrow strip leads to the particularly interesting conclusion that the impedance presented by the square depends only on its thickness. This qualitative result is supported by experiment. In the case of a disk resonator in a uniform field, the agreement is quantitative thanks to the greater accuracy of our approximation to the eigenfunction. The special cases studied are presented mainly as illustrative aids. The range of problems to which the formulation may be applied is considerably broader; we particularly wish to emphasize the applicability of these results when several modes are excited.

Appendix I

Orthogonality of Eigenfunctions: The orthogonality relation (5) is inspired by that of Walker [4]. However, the direction of M may vary throughout a generalized resonator so we need a slightly different derivation. By definition,

$$j\omega_u \Psi_u = \gamma M_s \hat{a}_m \times [\nabla \mathscr{G} \nabla \cdot -(H_i/M_s)]\Psi_u \tag{A1}$$

so

$$j\omega_u \Psi_u^* \times \Psi_v = \gamma(M_s \boldsymbol{h}_{du}^* \cdot \Psi_v - H_i \Psi_u^* \cdot \Psi_v)\hat{a}_m \tag{A2}$$

where we have written the demagnetizing field $\nabla \mathscr{G} \nabla \cdot \Psi_u$ as $\boldsymbol{h}_{du}$. Interchanging indices and conjugating,

$$j\omega_v \Psi_u^* \times \Psi_v = \gamma(M_s \boldsymbol{h}_{dv} \cdot \Psi_u^* - H_i \Psi_u^* \cdot \Psi_v)\hat{a}_m. \tag{A3}$$

Thus

$$j(\omega_u - \omega_v) \int_V \Psi_u^* \times \Psi_v \cdot \hat{a}_m \, dV$$

$$= \gamma M_s \int_V (\boldsymbol{h}_{du}^* \cdot \Psi_v - \boldsymbol{h}_{dv} \cdot \Psi_u^*) \, dV. \tag{A4}$$

The integral on the right-hand side vanishes for the reasons given by Walker, so

$$\int \Psi_u^* \times \Psi_v \cdot \hat{a}_m \, dV = 0, \qquad \text{for } \omega_u \neq \omega_v. \tag{A5}$$

Appendix II

To prove

$$\int_\Omega (\boldsymbol{m} + \boldsymbol{h}) \cdot \boldsymbol{h}_d \, dV = 0 \tag{B1}$$

we start with the observation that $\boldsymbol{h}_d$ is a gradient:

$$\boldsymbol{h}_d = \nabla\phi_d. \tag{B2}$$

Then from the divergence theorem

$$\int_\Omega (\boldsymbol{m}+\boldsymbol{h})\cdot\boldsymbol{h}_d\,dV = \int_{S_\Omega} \phi_d(\boldsymbol{m}+\boldsymbol{h})\cdot d\boldsymbol{S} - \int_\Omega \phi_d \nabla\cdot(\boldsymbol{m}+\boldsymbol{h})\,dV. \tag{B3}$$

The first integral on the right-hand side is zero because the RF magnetic induction $(\boldsymbol{m}+\boldsymbol{h})$ must be parallel to the coupling conductors, which define the surface S_Ω. The second integral is zero because $\nabla\cdot(\boldsymbol{m}+\boldsymbol{h}) = 0$.

A similar argument demonstrates that

$$\int_\Omega \boldsymbol{h}_e\cdot\boldsymbol{h}_d\,dV = 0. \tag{B4}$$

Acknowledgment

Thanks go to T. Ketcher for technical assistance, to R. Hiskes for supplying epitaxial YIG material, and to R. Engelmann for helpful discussions and criticism.

References

[1] R. W. DeGrasse, "Low-loss gyromagnetic coupling through single crystal garnets," *J. Appl. Phys.*, vol. 30, pp. 155S–156S, Apr. 1959.
[2] P. S. Carter, Jr., "Magnetically-tunable microwave filters using single-crystal Yttrium-iron-garnet resonators," *IRE Trans. Microwave Theory Tech.*, vol. MTT-9, pp. 252–260, May 1961. Also, P. S. Carter, Jr., and G. L. Matthaei, "Design criteria for microwave filters and coupling structures," Stanford Research Institute, Menlo Park, CA, Tech. Rep. 8, SRI Project 2326, Contract DA36-039-C-74862, Sept. 1959.
[3] M. Sparks, "Ferromagnetic resonance in thin films. I. Theory of normal mode frequencies," *Phys. Rev.*, vol. 1B, pp. 3831–3856, May 1970.
[4] L. R. Walker, "Magnetostatic modes in ferromagnetic resonance," *Phys. Rev.*, vol. 105, pp. 390–399, Jan. 1957.
[5] J. F. Dillon, Jr., "Magnetostatic modes in disks and rods," *J. Appl. Phys.*, vol. 31, pp. 1605–1614, Sept. 1960.
[6] B. A. Auld, "Walker modes in large ferrite samples," *J. Appl. Phys.*, vol. 31, pp. 1642–1647, Sept. 1960.
[7] N. Bloembergen, "Magnetic resonance in ferrites," *Proc. IRE*, vol. 44, pp. 1259–1269, Oct. 1956.
[8] P. S. Carter, Jr., "Equivalent circuit of orthogonal-loop-coupled magnetic resonance filters and bandwidth narrowing due to coupling inductance," *IEEE Trans. Microwave Theory Tech.*, vol. MTT-18, pp. 100–105, Feb. 1970.
[9] M. Sparks, "Magnetostatic modes in an infinite circular disk," *Solid State Commun.*, vol. 8, pp. 731–733, 15 May 1970.

Further Studies on the Microwave Auditory Effect

JAMES C. LIN, SENIOR MEMBER, IEEE

Abstract—**Auditory signals generated in humans and animals who are irradiated with short rectangular pulses of microwave energy have been studied. Assuming that the effect arises from sound waves generated in the tissues of the head by rapid thermal expansion caused by microwave absorption, and using a technique described previously, the governing equations are solved for a homogeneous spherical model of the head under constrained-surface conditions. The results indicate that the frequency of the auditory signal is a function of the size and acoustic property of the head only. While the amplitude and frequency of the microwave-induced sound are higher than those predicted by the stress-free boundary condition formulation, they are compatible with the experimental results reported to date.**

Introduction

IN RECENT YEARS many investigators have studied the auditory sensations produced in man by appropriately modulated microwave energy [1]–[5]. Other investigators [3], [5]–[7] have shown that electrophysiologic auditory activity may be evoked by irradiating the brains of laboratory animals with rectangular pulses of microwave energy. Responses elicited in cats both by conventional acoustic stimuli and by pulsed microwaves were similar and they disappeared following disablement of the cochlea and following death. More recently, cochlear microphonics have been recorded from the round window of cats and guinea pigs during irradiation by pulse-modulated 918-MHz microwaves. These results suggested that microwave-induced auditory sensation is transduced by a mechanism similar to that responsible for conventional sound perception and that the primary site of interaction resides somewhere peripheral to the cochlea. A peripheral response to microwave pulses should involve mechanical displacement of the tissues of the head with resultant dynamic effects on the cochlea.

Several physical mechanisms have been suggested to account for the conversion of microwaves to acoustic energies; these include radiation pressure, electrostriction, and thermal expansion [3], [8]–[10]. A comparison of these three mechanisms for planar geometries revealed that the forces of

Manuscript received October 26, 1976; revised April 4, 1977. This work was supported in part by National Science Foundation under Grant ENG 75-15227.

The author is with the Department of Electrical and Computer Engineering and the Department of Physical Medicine and Rehabilitation, Wayne State University, Detroit, MI 48202.